Electron transport nonlocality in monolayer graphene modified with hydrogen silsesquioxane polymerization

A. A. Kaverzin* and B. J. van Wees

Physics of Nanodevices, Zernike Institute for Advanced Materials, University of Groningen, Groningen, The Netherlands

(Received 18 February 2015; revised manuscript received 20 March 2015; published 13 April 2015)

A number of practical and fundamental applications of graphene requires modification of some of its properties. In this paper we study the effect of polymerization of a hydrogen silsesquioxane film on top of monolayer graphene with the intent to increase the strength of the spin-orbit interaction. The measured nonlocal resistances R_{NL} were found to be up to 700 Ω, significantly exceeding the expected contribution from conventional Ohmic currents. The R_{NL} dependence on the channel length resembles exponential decay with a characteristic length of $\lambda \simeq 500$ nm that is close to the spin-relaxation length in graphene reported elsewhere. The sensitivity of the measured effect to the electron-beam exposure was shown to decrease with an increased level of the surface contamination. However, no modulation of the effect is observed when an in-plane magnetic field is applied. This implies that a spin Hall model fails to explain the observed phenomenon and an alternative interpretation is required.

DOI: 10.1103/PhysRevB.91.165412 PACS number(s): 72.25.−b, 72.80.Vp, 75.40.Gb, 75.70.Tj

I. INTRODUCTION

The present understanding of graphene physics allows researchers to look beyond conventional charge and heat transport properties and explore more subtle electronic characteristics, such as the spin and pseudospin degrees of freedom. In order to study these properties one has to have suitable mechanisms for creation, manipulation, and detection of such spin or pseudospin currents. For example, for spin the most common techniques imply the usage of the charge current and its conversion by ferromagnets into spin currents [1,2]. Effective conversion between spin and charge currents can be realized in a system with a large enough strength of the spin-orbit interaction [2]. Similarly, the valley Hall effect can be used for a controllable conversion between charge and valley currents and is expected to arise in a system with broken inversion symmetry in the crystal structure [3,4].

In pristine graphene the theoretically predicted spin-orbit interaction is negligibly small [5], and that is exactly why graphene is seen as a potentially optimal medium for spin manipulation. Absence of spin-orbit interaction ensures high spin relaxation times which, along with high electron mobility, give large spin-relaxation lengths. At the same time it was suggested that the hydrogenation of graphene is a promising option for spin injection and detection [2]. Hydrogenated graphene has been intensively explored theoretically as it offers valuable modifications of graphene properties depending on the coverage of the surface. In the high coverage limit hydrogenated graphene was predicted [6–9] and later confirmed experimentally [10–12] to reveal an insulating behavior, appealing to the usage of graphene in semiconductor devices. In the low coverage limit hydrogen adatoms are thought to introduce an additional spin-orbit interaction [13,14], thus, expanding graphene ubiquity into the realm of spin manipulation. In this regime enhanced spin-orbit coupling gives rise to interchangeable conversion between the charge and the spin currents, thus, bringing direct and inverse spin Hall effects into an experimentally observable range.

In this paper we modify Hall bar-shaped graphene samples by covering them with a hydrogen silsesquioxane (HSQ) film. Exposure of this film with high-energy electrons causes the release of hydrogen due to polymerization of HSQ and can potentially result in graphene hydrogenation as shown in Ref. [15]. Experimentally, after the sample modification we found a significant increase in the measured nonlocal signal that cannot account for an Ohmic charge current contribution. We study this phenomenon by varying the sample geometry, by changing the exposure dose, and by applying the magnetic field. Our findings suggest that the observed nonlocal transport cannot be explained by the charge or heat transport models and is, therefore, mediated by a nontrivial current state. However, the absence of in-plane magnetic-field influence on the measured nonlocal signal argues against the spin nature of the effect, thus, leaving the origin of the observed phenomenon as an open question.

II. SAMPLE FABRICATION

Samples were made out of graphene flakes exfoliated on top of n^+ Si/SiO_2 wafers with a 300-nm oxide layer. The single-layer flakes were selected initially by optical contrast, and later their thickness was confirmed with Raman spectroscopy [16] and/or quantum Hall effect [17,18]. Everywhere below in the text we will be discussing monolayer graphene unless specified otherwise. The graphene was contacted with multiple Ti/Au electrodes fabricated via electron-beam (e-beam) lithography with the use of a polymethyl methacrylate (PMMA) resist. Another lithography step was performed for the preparation of a Hall bar mask on top of the flake. Either PMMA or HSQ (FOX-16 Dow Corning Co.) was used as a resist for patterning the mask. The uncovered graphene parts were removed by oxygen plasma. Three types of samples A, B, and C were fabricated in order to distinguish between different initial states of the interface between the graphene flake and the HSQ film or mask. For A-type samples, first, the contacts were deposited, and then the Hall bar mask was made in the HSQ film followed by etching. B-type samples were etched with a mask made from PMMA after the contact deposition,

*a.kaverzin@rug.nl

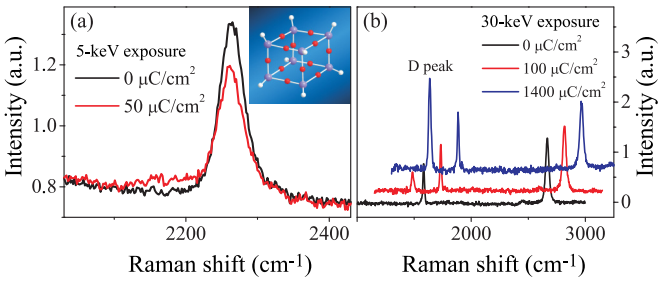

FIG. 1. (Color online) (a) Raman spectra of the HSQ film both on top of the graphene and away from it before (black curve) and after (red curve) the exposure. The intensity is normalized to the intensity of the G peak for both curves. The inset shows a schematic of the HSQ monomer. Silicon atoms are shown with purple filled circles, oxygen with red filled circles, and hydrogen with white filled circles. (b) Raman spectra of the graphene sample covered with the HSQ film after successive exposures with an electron beam. Red and blue curves are shifted both horizontally and vertically for clarity.

and only then was the sample uniformly covered with HSQ. Finally, samples of type C were coated with HSQ directly after exfoliation in order to minimize the contamination level of the graphene-HSQ interface. For this type the Hall bar mask was defined in the first lithography step in HSQ, then it was coated with PMMA followed by the second lithography step and metal deposition, and only then the sample was etched. Determined by lithography the geometry of the samples was confirmed with scanning electron microscopy (SEM) imaging with accuracy better than ~10%. In total seven samples (three A samples, one B sample, and three C samples) were measured and showed a consistent behavior.

The graphene conducting channels were functionalized with the help of an electron-beam exposure of the HSQ mask or film that was formed on top of the device. Hydrogen silsesquioxane is known as a high-resolution negative tone resist [19]. Its monomer has a cubic shape with Si atoms in the corners that are linked with oxygen atoms; see the inset to Fig. 1(a). The remaining silicon bonds are saturated with hydrogen. When an HSQ film is exposed with the electron-beam, SiH bonds get dissociated, and neighboring monomers cross-link via an extra oxygen atom. At the same time released hydrogen becomes available for covalently bonding to the graphene surface [15,19]. Scission of the SiH bond leads to the modification of the vibration modes of the HSQ film and can be detected via Raman spectroscopy. Moreover, when bonding to graphene, hydrogen locally modifies the hybridization from sp^2 to sp^3, therefore, introducing an atomic-scale imperfection in the lattice of the crystal [7]. Such imperfections are known to cause intervalley scattering of the carriers and result in the appearance of a D peak in the Raman spectrum of graphene [16,20].

III. RAMAN SPECTROSCOPY AND NONLOCAL TRANSPORT CHARACTERIZATION

We used Raman spectroscopy to confirm the effect of the electron-beam exposure on the HSQ-graphene system and to relate the used doses to the reported values in Refs. [2,15]. In the spectrum of the HSQ film we were able to identify a peak around 2260 cm^{-1} that is associated with the presence of SiH bonds [21]; see Fig. 1(a). The normalized intensity of this peak was seen to prominently decrease after exposure with an e-beam, thus, confirming the hydrogenation model proposed in Ref. [15]. Besides, after the first e-beam irradiation the Raman spectrum of graphene showed an appearing D peak which continued to increase in relative intensity with further exposures; see Fig. 1(b). The intensity of the D peak was found to grow monotonically with irradiation implying a monotonic increase in the hydrogen coverage [15]. Using the relation between the defect concentration and the relative intensity of the D peak I_D/I_G [22] we estimated the coverage of the defects as 0.006% and 0.02% for 100 and 1400 $\mu C/cm^2$, respectively. The strength of the induced spin-orbit coupling is expected to depend linearly on the level of functionalization, thus, suggesting in a certain range of exposures monotonic and close-to-linear relations between the relative intensity of the D peak and the strength of the spin-orbit interaction.

To study the effect of such a modification on charge transport in our graphene samples, we used a Hall bar geometry; see Fig. 2. Employment of a nonlocal measurement scheme allowed us to separate the classical Ohmic consequences of the charge transport from the studied phenomenon. In a system with the enhanced spin-orbit interaction, a drifting electron is scattered into the direction that depends on the spin. For a Hall bar geometry it implies that an applied transverse charge current I_q results in a longitudinal spin current (spin Hall effect) I_M that diffuses over relatively long distances in a longitudinal direction. In turn, spin current is converted back into the charge current (inverse spin Hall effect), which is detected as a builtup transverse voltage difference V_{NL}. From here we will use the notation of a nonlocal resistance R_{NL}, which is defined as V_{NL}/I_q and is a measure of the conversion efficiency between I_M and I_q. The axis of spin quantization is

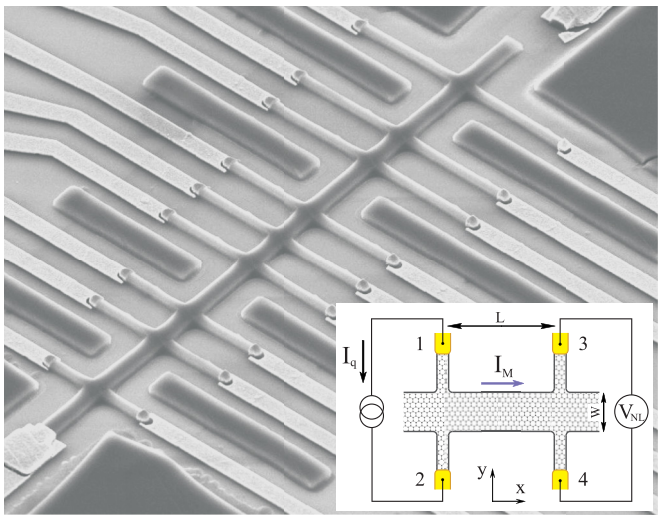

FIG. 2. (Color online) SEM image of sample $C2$ under a 45° angle. The scale is given by the width of the channel, which is 0.5-μm wide. The inset: schematic of the measuring circuit and the measured region of the sample. The transverse charge current I_q between electrodes 1 and 2 is converted into the mediative current I_M and then converted back into the voltage drop between 3 and 4.

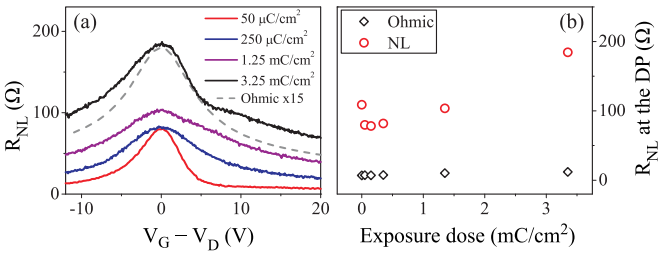

FIG. 3. (Color online) (a) The nonlocal resistance of sample $A1$ plotted as a function of $V_G - V_D$ [where V_D is the Dirac point (DP) position] for different 30-keV exposures. The Ohmic contribution corresponding to the highest dose is given as a dashed line and is scaled up by 15 times. $L = 2$, $W = 1$ μm. (b) R_{NL} (red empty circles) at the Dirac point for the curves shown in panel (a) along with the corresponding values of R_{Ohmic} (black empty diamonds) plotted against the exposure dose.

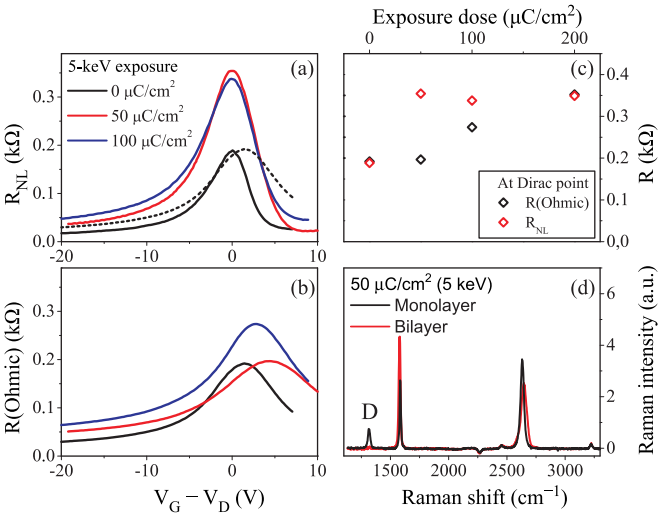

FIG. 4. (Color online) (a) R_{NL} as a function of the gate voltage for sample $B1$ after successive exposures. The dashed line gives $R_{\text{Ohmic}}(V_G)$ dependence for an initial unexposed state. (b) $R_{\text{Ohmic}}(V_G)$ dependences corresponding to the curves in panel (a). (c) R_{NL} (red empty diamonds) at the Dirac point along with the corresponding values of R_{Ohmic} (black empty diamonds) plotted against the exposure dose. (d) Raman spectra of the monolayer (black curve) and bilayer (red curve) graphene samples covered with HSQ after 50-μC/cm^2 exposure.

determined by both the sample geometry and the direction of I_q and is perpendicular to the graphene plane.

In Fig. 3(a) nonlocal resistance is plotted as a function of the gate voltage for sample $A1$. Solid curves of different colors correspond to different states of the sample after successive e-beam exposures. The dashed gray line shows the calculated Ohmic contribution R_{Ohmic} for a final state with the highest exposure level. It is approximated by the formula [23],

$$R_{\text{Ohmic}} = \frac{4}{\pi}\rho \exp(-\pi L/W), \tag{1}$$

that is valid for $L/W \gtrsim 1$, where ρ is the sample resistivity and W and L are the width and the length of the channel, respectively. Sample resistivity was measured with a four-terminal technique at all stages of the experiment. The relation Eq. (1) is derived with an assumption of an infinitely long conductor and infinitely thin contact electrodes that are placed exactly opposite to each other in a Hall bar. We studied the influence of a finite electrode width and a geometry inaccuracy of their positioning on the value of R_{Ohmic} with a simple COMSOL simulation of the classical current distribution in a two-dimensional conductor. Replication of the real sample geometry resulted in a less than 15% deviation from the value calculated with Eq. (1), thus, justifying its applicability.

From Fig. 3(a) one can clearly see that there is an order of magnitude difference between the measured R_{NL} and the corresponding R_{Ohmic}, meaning that the observed nonlocal signal cannot be explained by a trivial Ohmic component. To track the magnitude of R_{NL} with increasing exposure we replotted the value of nonlocal resistance at the Dirac point as a function of the dosage Q; see Fig. 3(b). The relation between R_{NL} and exposure dose is seen to be monotonically increasing in the studied range except in the vicinity of $Q = 0$. The initial decrease in R_{NL} does not fit within a simple spin Hall effect model, and its explanation might require an inclusion of other related side effects of the graphene functionalization. Away from the Dirac point the behavior of the nonlocal resistance is quantitatively similar to that shown in Fig. 3(b).

The initial state of the sample shown in Fig. 3(a) corresponds to a zero exposure, however, the nonlocal resistance in this state was already significantly larger than the corresponding Ohmic contribution. This can be explained by the fact that the shown initial state is not truly the unexposed state since during the mask fabrication the HSQ layer was already irradiated with the 50-μC/cm^2 dose at 5 keV (Sec. II). To prove this assumption, we prepared B-type samples where the preliminary exposure of HSQ was excluded by making the Hall bar mask with the PMMA resist. Therefore, the initial state of the HSQ film was truly unexposed before the measurements. In Fig. 4(a) we show the nonlocal resistance for sample $B1$ for both an unexposed state and after a set of exposures. The corresponding Ohmic contributions are given in panel (b). The magnitude of the nonlocal signal in the unexposed sample turned out to be of the same order as the Ohmic contribution, thus, providing more evidence that the observed effect is directly related to the HSQ film on top of the graphene being affected by the electron irradiation.

Comparing Figs. 3(a), 3(b), 4(a), and 4(c) one can notice that the sensitivities of samples $A1$ and $B1$ differ significantly, meaning that similar dosage results in a smaller effect in sample $B1$. Moreover, for sample $B1$ the nonlocal resistance saturates after 200 μC/cm^2 in a sense that it becomes of the order of the Ohmic contribution; see Fig. 4(c), whereas for sample $A1$, R_{NL} keeps increasing in a range up to 3 mC/cm^2. Such a prominent difference most likely comes from the contamination level of the interface between the graphene and the HSQ film. The fact is that while preparing sample $B1$, the PMMA resist was spun twice on the surface of the sample for the electrodes' lithography and for the Hall bar mask. PMMA is known to leave a significant amount of residue on the graphene surface [24–26] and, therefore, its multiple usage might reduce the clean surface of graphene available for the hydrogen bonding. Furthermore, in the case of sample $B1$ the irradiation was performed with 5-kV acceleration voltage

(the same voltage was used for defining the mask in HSQ), whereas sample $A1$ was exposed with 30-kV electrons. The energy of the electrons influences the scattering probability of the propagating electron, thus, potentially contributing to the difference in the sensitivity for samples $A1$ and $B1$.

Further comparison between the exposures with low- and high-energy electrons can be performed with Raman spectroscopy. Namely, in Fig. 4(d) the spectrum of the graphene-HSQ system is shown after 50-μC/cm^2 exposure with a 5-kV acceleration voltage. Comparing the relative intensity of the D peak with the spectra given in Fig. 1(b) for 30 kV, we conclude that irrespective of the electron energy the amount of produced hydrogen bonds is of the same order of magnitude for similar doses. Thus, we eliminate the influence of the acceleration voltage on the hydrogenation process and conclude that a significant difference in the saturation doses for samples $A1$ and $B1$ is likely to be associated with the surface contamination by the PMMA residues.

Along with the Raman spectrum of an exposed monolayer graphene-HSQ interface, we measured the Raman spectrum of the exposed bilayer graphene-HSQ interface; see Fig. 4(d). As is seen, the D peak in the spectrum of bilayer graphene is practically absent indicating insensitivity in a given exposure range of the bilayer graphene-HSQ interface to the hydrogenation process [15].

At last we studied dependence of the nonlocal resistance on the distance between injecting and detecting electrodes L. In Fig. 5 R_{NL} as a function of the gate voltage is plotted for different L's for two samples $C1$ and $C2$. R_{NL} for sample $C1$ is plotted with black empty squares, red empty circles, and blue empty triangles for $L = 1$–3 μm, respectively ($W = 1$ μm). Nonlocal signals measured in sample $C2$ are plotted with red empty diamonds and gray empty diamonds for $L = 1,2$ μm, respectively ($W = 0.5$ μm). The dashed lines give corresponding calculated Ohmic contributions for each dashed curve. A consistent linear decrease in the R_{NL} on a logarithmic scale with the increasing channel length suggests

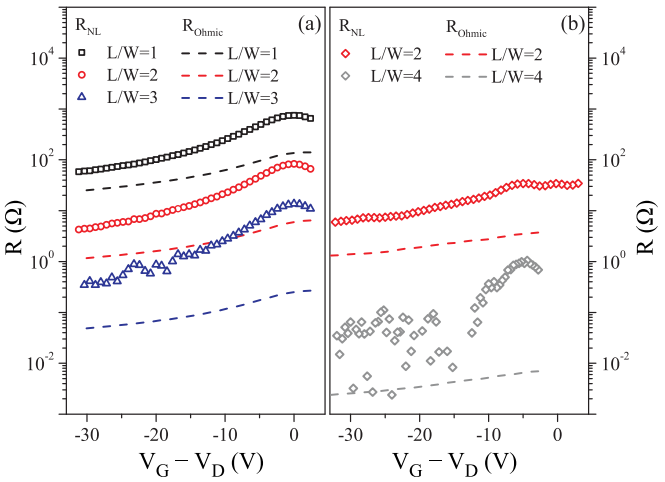

FIG. 5. (Color online) (a) R_{NL} as a function of the gate voltage. Different curves correspond to different L/W ratios for sample $C1$. The dashed lines give the corresponding calculated Ohmic contribution $T = 4.2$ K. (b) Nonlocal resistance as a function of gate voltage for different L/W ratios for sample $C2$.

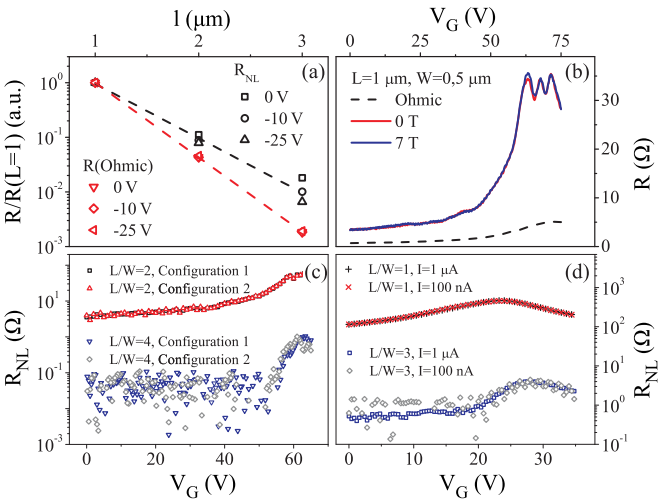

FIG. 6. (Color online) (a) R_{NL} (black empty squares, circles and triangles) and R_{Ohmic} (red empty diamonds and triangles) at the different carrier concentrations (gate voltages) are plotted as a function of the channel length for sample $C1$. The dashed lines show an exponential fit with Eqs. (2) and (1) for R_{NL} and R_{Ohmic}, respectively. (b) Nonlocal resistance for sample $C2$ measured with $B = 0$ T (red line) and $B = 7$ T (blue line) in-plane magnetic field. The dashed line represents the corresponding $R_{\text{Ohmic}}(V_G)$ dependence. (c) $R_{NL}(V_G)$ dependences for the reciprocal current injection/detection circuits for sample $C2$. Configuration 1: I_q is applied between the contacts 1 and 2 (see Fig. 2), and V_{NL} is measured between the contacts 3 and 4. Configuration 2: I_q is between 3 and 4, and V_{NL} is measured between 1 and 2. (d) $R_{NL}(V_G)$ dependences for different magnitudes of the I_q current for sample $C1$.

an exponential dependence of the nonlocal signal on L. In theory, following the spin Hall model the nonlocal resistance should obey the analytical expression [23],

$$R_{NL} = \frac{1}{2}\gamma^2 \rho \frac{W}{\lambda_s} \exp\left(-\frac{L}{\lambda_s}\right), \tag{2}$$

where γ is a spin Hall angle or efficiency of conversion between the spin and the charge currents and λ_s is a spin-relaxation length. This means that for $W < \pi\lambda_s$ the nonlocal resistance should decay with the distance slower than the Ohmic contribution, thus, enhancing the difference between the two. After replotting R_{NL} for sample $C1$ as a function of L for three different gate voltages we were able to fit the data with Eq. (2) and extract the characteristic length; see Fig. 6(a). λ_s was found to be in the range of 400–700 nm depending on the carrier concentration. At the Dirac point the characteristic length was found to be longer than that at higher concentrations.

IV. EFFECT OF THE IN-PLANE MAGNETIC FIELD

So far, all our findings support the proposed spin Hall model in Refs. [2,23]. Namely, behavior of the nonlocal resistance with an increase in the exposure dose and with enlarging the channel length can be consistently explained within the limits of the model. The extracted characteristic length of 440 nm is also close to the values reported elsewhere for the spin-relaxation length in the low quality graphene samples

[27,28]. However, when taking a step further in the analysis and calculating the spin Hall angle with Eq. (2) we obtained an unrealistically high value of $\gamma \approx 1.5$. Basically, this discrepancy can be interpreted as if the measured nonlocal signal is higher than its analytical estimate within an assumption of 100% conversion between the charge and the spin currents (equivalently $\gamma = 1$).

Another discrepancy with the spin Hall model is revealed when we consider the width W dependence of the nonlocal resistance. The extracted characteristic length λ_s for sample $C2$ was found to be close to that in sample $C1$. This means that R_{NL} should change linearly with W from sample $C1$ to sample $C2$ if L is kept constant and if the resistivities of the two samples are similar (which is the case). However, from Fig. 5 we see that for the same channel length (for example, red empty circles for $C1$ and gray empty diamonds for $C2$) the two orders of magnitude change in nonlocal resistance cannot be accounted by the two times change in W and at most two times change in resistivity. It is more likely that R_{NL} scales down with the L/W ratio rather than with L/λ_s.

Moreover, the spin-mediated nonlocal transport is supposed to be sensitive to the applied in-plane magnetic field B. In particular, the Larmor precession in such a field should result in the modulation of R_{NL} with suppression of the signal down to zero at a high enough field. This phenomenon is well known and is often referred to as the Hanle effect. Along with Eq. (2) one can derive a modified expression for R_{NL} in the presence of the in-plane magnetic field. In the limit of strong magnetic fields ($\omega_B \tau_s \gg 1$) the expression reads [23]

$$R_{NL}(L) = \frac{1}{\sqrt{2}} \gamma^2 \rho \eta \frac{W}{\lambda_s} \sin\left(\frac{\eta L}{\lambda_s} + \frac{\pi}{4}\right) \exp\left(-\frac{\eta L}{\lambda_s}\right), \quad (3)$$

where $\eta = \sqrt{\omega_B \tau_s}$, $\omega_B = g \mu_B B$, g is the g factor of electrons, μ is the Bohr magneton, τ_s is a spin-relaxation time given by $\tau_s = \lambda_s^2 / D_s$, and D_s is a diffusion coefficient. Using this equation one can estimate the values of the field $B_{R_{NL}=0}$ when R_{NL} crosses the zero level. These calculations require the value of D that can be estimated from the resistivity dependence on the gate voltage. For $L/\lambda_s = 1$ we get that R_{NL} crosses zero when $\omega_B \tau_s \simeq 2$. Using values for D and λ_s we estimate $B_{R_{NL}=0} \simeq 2$ T. Therefore, for $L/\lambda_s = 2$ in the field range up to 2 T we should see a decrease in the nonlocal signal down to zero and further oscillation with exponentially decaying amplitude. However, experimentally in disagreement with the predictions of the spin Hall model we observe no significant change in R_{NL} with the applied in-plane magnetic field up to 7 T. It is illustrated in Fig. 6(b) as the nonlocal signal for both $B = 0$ T (in red) and $B = 7$ T (in blue) for sample $C2$ at 4,2 K. This observation gives a strong argument against the proposed model of the spin-mediated nonlocal transport and is drastically different from the reported results in Ref. [2], although we tried to follow the described fabrication procedure as close as possible. A possible quantitative difference could be expected from the sensitivity of the nonlocal signal to the level of interface contamination.

V. DISCUSSIONS AND CONCLUSIONS

The major part of our results can be ascribed to the model proposed in the literature of the spin-mediated nonlocal transport in hydrogenated graphene. However, the magnetic-field inability to modulate the value of R_{NL} disproves the spin origin of the mediative current. It puts these findings into a contradiction with already reported results on hydrogenated graphene and suggests looking for an alternative mechanism that can account for the observed nonlocal effect.

In Ref. [29] it was reported that a significant contribution to the first-harmonic nonlocal signal can arise from the magnetothermoelectric effects. However, our samples were found to obey reciprocity indicating the absence of any intrinsic magnetic field in the system; see Fig. 6(c). Moreover, we exclude from the consideration temperature-related mechanisms by showing that the measured resistance does not change with the applied current except that the signal-to-noise ratio gets improved; see Fig. 6(d).

Electrons in graphene possess not only a spin degree of freedom, but also a pseudospin relating them to the different valleys of the band structure. It was reported recently that if the symmetry between the A and the B sublattices in monolayer graphene is broken by the proximity to the matched lattice of the boron nitride, it is reasonable to expect the appearance of the nonlocal transport mediated by the valley current. However, the results published in Ref. [3] showed behavior different from what we observe. In particular R_{NL} was found to depend strongly on temperature indicating activated behavior. In our samples with temperature lowered from room temperature down to 4 K we did not see any significant modulation of R_{NL} except for an appearance of the universal conductance fluctuation oscillations. Moreover, the key ingredient for the appearing valley-mediated current is a homogeneous asymmetry between the two sublattices. Such asymmetry can be obtained in the van der Waals structure of graphene and boron nitride, but it is highly unlikely for the released hydrogen to bond to the graphene in an ordered fashion.

Summing up, we observed reproducibly and consistently a nonlocal resistance in a number of different samples fabricated in three distinguished ways. We showed that the measured values of R_{NL} cannot be explained by an ordinary charge transport effect and has to be assigned to a mediative mechanism of nontrivial origin with a characteristic length of $\sim$500 nm. The spin-related explanation proposed in the literature cannot be used for our results since an in-plane magnetic field was found to have no effect on the observed values. We also excluded temperature-related mechanisms and showed that the valley currents are unlikely to be the origin of the effect. Our findings suggest that future studies of nonlocal effects in graphene-HSQ systems can be complicated by an effect of unknown origin, such as observed in this paper.

ACKNOWLEDGMENTS

We would like to thank M. de Roosz, H. Adema, and J. G. Holstein for technical support and I. J. Vera-Marun for useful discussions and reading the paper. This work was financially supported by the Dutch Foundation for Fundamental Research on Matter (FOM), the Zernike Institute for Advanced Materials, and the European Union Seventh Framework Programme under "Graphene Flagship" (Grant No. 604391).

[1] W. Han, R. K. Kawakami, M. Gmitra, and J. Fabian, Nat. Nanotechnol. **9**, 794 (2014).
[2] J. Balakrishnan, G. Kok Wai Koon, M. Jaiswal, A. H. Castro Neto, and B. Ozyilmaz, Nat. Phys. **9**, 284 (2013).
[3] R. V. Gorbachev, J. C. W. Song, G. L. Yu, A. V. Kretinin, F. Withers, Y. Cao, A. Mishchenko, I. V. Grigorieva, K. S. Novoselov, L. S. Levitov *et al.*, Science **346**, 448 (2014).
[4] K. F. Mak, K. L. McGill, J. Park, and P. L. McEuen, Science **344**, 1489 (2014).
[5] D. Huertas-Hernando, F. Guinea, and A. Brataas, Phys. Rev. B **74**, 155426 (2006).
[6] J. O. Sofo, A. S. Chaudhari, and G. D. Barber, Phys. Rev. B **75**, 153401 (2007).
[7] D. W. Boukhvalov, M. I. Katsnelson, and A. I. Lichtenstein, Phys. Rev. B **77**, 035427 (2008).
[8] L. A. Chernozatonskiĭ, P. B. Sorokin, E. É Belova, J. Brüning, and A. S. Fedorov, JETP Lett. **85**, 77 (2007).
[9] S. Casolo, O. M. Løvvik, R. Martinazzo, and G. F. Tantardini, J. Chem. Phys. **130**, 054704 (2009).
[10] D. C. Elias, R. R. Nair, T. M. G. Mohiuddin, S. V. Morozov, P. Blake, M. P. Halsall, A. C. Ferrari, D. W. Boukhvalov, M. I. Katsnelson, A. K. Geim *et al.*, Science **323**, 610 (2009).
[11] R. Balog, B. Jorgensen, L. Nilsson, M. Andersen, E. Rienks, M. Bianchi, M. Fanetti, E. Laegsgaard, A. Baraldi, S. Lizzit *et al.*, Nat. Mater. **9**, 315 (2010).
[12] A. Castellanos-Gomez, M. Wojtaszek, Arramel, N. Tombros, and B. J. van Wees, Small **8**, 1607 (2012).
[13] A. H. Castro Neto and F. Guinea, Phys. Rev. Lett. **103**, 026804 (2009).
[14] M. Gmitra, D. Kochan, and J. Fabian, Phys. Rev. Lett. **110**, 246602 (2013).
[15] S. Ryu, M. Y. Han, J. Maultzsch, T. F. Heinz, P. Kim, M. L. Steigerwald, and L. E. Brus, Nano Lett. **8**, 4597 (2008).
[16] A. C. Ferrari, J. C. Meyer, V. Scardaci, C. Casiraghi, M. Lazzeri, F. Mauri, S. Piscanec, D. Jiang, K. S. Novoselov, S. Roth *et al.*, Phys. Rev. Lett. **97**, 187401 (2006).
[17] K. S. Novoselov, A. K. Geim, S. V. Morozov, D. Jiang, M. I. Katsnelson, I. V. Grigorieva, S. V. Dubonos, and A. A. Firsov, Nature (London) **438**, 197 (2005).
[18] Y. Zhang, Y.-W. Tan, H. L. Stormer, and P. Kim, Nature (London) **438**, 201 (2005).
[19] H. Namatsu, Y. Takahashi, K. Yamazaki, T. Yamaguchi, M. Nagase, and K. Kurihara, J. Vacuum Sci. Technol. B **16**, 69 (1998).
[20] A. C. Ferrari and D. M. Basko, Nat. Nanotechnol. **8**, 235 (2013).
[21] P. Bornhauser and G. Calzaferri, J. Phys. Chem. **100**, 2035 (1996).
[22] L. G. Cancado, A. Jorio, E. H. M. Ferreira, F. Stavale, C. A. Achete, R. B. Capaz, M. V. O. Moutinho, A. Lombardo, T. S. Kulmala, and A. C. Ferrari, Nano Lett. **11**, 3190 (2011).
[23] D. A. Abanin, A. V. Shytov, L. S. Levitov, and B. I. Halperin, Phys. Rev. B **79**, 035304 (2009).
[24] A. Pirkle, J. Chan, A. Venugopal, D. Hinojos, C. W. Magnuson, S. McDonnell, L. Colombo, E. M. Vogel, R. S. Ruoff, and R. M. Wallace, Appl. Phys. Lett. **99**, 122108 (2011).
[25] Y.-C. Lin, C.-C. Lu, C.-H. Yeh, C. Jin, K. Suenaga, and P.-W. Chiu, Nano Lett. **12**, 414 (2012).
[26] M. Her, R. Beams, and L. Novotny, Phys. Lett. A **377**, 1455 (2013).
[27] C. Józsa, T. Maassen, M. Popinciuc, P. J. Zomer, A. Veligura, H. T. Jonkman, and B. J. van Wees, Phys. Rev. B **80**, 241403 (2009).
[28] T. Maassen, J. J. van den Berg, E. H. Huisman, H. Dijkstra, F. Fromm, T. Seyller, and B. J. van Wees, Phys. Rev. Lett. **110**, 067209 (2013).
[29] J. Renard, M. Studer, and J. A. Folk, Phys. Rev. Lett. **112**, 116601 (2014).